Infrared Chemiluminescence Study of the Reaction of Hydroxyl Radical with Acetaldehyde and the Secondary Reactions of Acetyl Radical with NO_2, OH, and H

Nadezhda I. Butkovskaya*,† and Donald W. Setser‡

Physikalische Chemie/FB9, Bergische Universität-GH Wuppertal, D-42097 Wuppertal, FRG, and Department of Chemistry, Kansas State University, Manhattan, Kansas 66506

Received: May 5, 2000; In Final Form: August 16, 2000

The hydrogen abstraction reactions from CH_3CHO by OH and OD radicals were studied in a fast-flow reactor by observation of the infrared chemiluminescence from H_2O and HOD. The fraction of available energy released as the vibrational energy of water was $\langle f_v \rangle = 0.52$ with ~30% released as bending excitation and ~65% released as stretching excitation of the newly formed OH bond. The pattern of energy disposal closely resembles that for OH + H_2CO or $(CH_3)_2S$ reactions, but differs from abstraction from secondary C−H bonds of hydrocarbons. Secondary reactions of CH_3CO radical with NO_2, OH, and H also were observed by infrared emission of products formed from the unimolecular decomposition of $CH_3C(O)ONO$, $CH_3C(O)OH$, and $CH_3C(O)H$ intermediate adducts. The CO_2 vibrational distributions from the decomposition of $CH_3C(O)OH$, $CH_3C(O)ONO$, and $HC(O)ONO$ are compared.

1. Introduction

As part of an effort to systematically study the energy disposal of H atom abstraction by OH radicals by infrared chemiluminescence (IRCL), we have already reported results for reactions with some hydrocarbons,[1] hydrogen halides,[1−3] and sulfides.[4] Abstraction from aldehydes presents the opportunity to characterize reactions with C−H bonds with larger exoergicity than secondary C−H bonds of alkanes. Formaldehyde and acetaldehyde are important intermediates in the oxidation of organic compounds. Particularly, the bimolecular reactions of these aldehydes and the relevant formyl (HCO) and acetyl (CH_3CO) radicals are involved in processes of low-temperature combustion and atmospheric photooxidation of hydrocarbons.[5,6] In recent work we have analyzed the vibrational excitation of H_2O and HOD molecules formed in the reactions of OH and OD radicals with formaldehyde, CH_2O.[7] The total vibrational energy, $\langle f_v \rangle \cong 0.57$, and the energy released into the newly formed O−H bond (63%) and into the bending mode (36%) were determined. In the present study, the infrared chemiluminescent spectra of the isotopic water molecules were measured and analyzed from the reactions of OH and OD radicals with acetaldehyde, CH_3CHO.

$$OH + CH_3C(O)H \rightarrow H_2O + CH_3CO \quad (1)$$

$$OD + CH_3C(O)H \rightarrow HOD + CH_3CO \quad (2)$$

The reactions took place in a fast-flow reactor that was observed by a Fourier transform infrared spectrometer. The fast H(D) + NO_2 → OH + NO reaction was used in a prereactor as the source of OH(OD) radicals. OH(OD) + $CH_3C(O)H$ is a convenient chemical system to study the secondary reactions of CH_3CO radical with H, OH, NO, and NO_2. Infrared emission was observed from water, the primary product, and CO_2, CO, and HNO from the secondary reactions.

The energy available for products of reaction 1 can be obtained from the equation $\langle E_{av} \rangle = -\Delta H_0^\circ + 4RT + E_a$, where E_a is the activation energy and ΔH_0° is the reaction enthalpy. The thermodynamic and kinetic data for the reactions involved in the study are presented in Table 1. The enthalpy of reaction 1 is $\Delta H_0^\circ = -30.2$ kcal mol^{-1}, as calculated from the bond energies of $D_0(CH_3CO-H) = 87.9$ kcal mol^{-1} and $D_0(HO-H) = 118.08$ kcal mol^{-1}.[14] The available energy for reaction 1 is 32.6 kcal mol^{-1}, which is sufficient to excite up to three stretching quanta and up to six bending quanta of the water molecule. The vibrational distributions for the primary H_2O and HOD products were obtained by simulation of the H_2O and HOD spectra under conditions free of secondary reactions and vibrational relaxation. Comparison with the results from CH_2O shows that the energy disposals to H_2O and HOD are very similar, but rather different from abstraction of H atoms from secondary C−H bonds of hydrocarbons.

The secondary reactions of CH_3CO radical with NO_2, OH, and H are also sufficiently exothermic (see Table 1) to give vibrationally excited products, and CO_2, CO, and HNO emission was observed. The spectra of the CO_2 molecules from NO_2 + CH_3CO and OH + CH_3CO reactions were also analyzed by computer simulation and compared, respectively, with the CO_2 spectra from NO_2 + HCO reaction and unimolecular decomposition of acetic acid. The possible sources of CO and HNO, which could be both the direct secondary reactions of acetyl with H and NO and the tertiary reactions of HCO radical with H and NO, are discussed.

2. Experimental Methods

2.1. Experimental Setup. The experimental methods used to observe the vibrational excitation of products from fast gas-phase chemical reactions have been previously described.[7,15] In the present work, the infrared chemiluminescence spectra from vibrationally excited H_2O, CO_2, and CO molecules were

† Bergische Universität-GH Wuppertal. E-mail: nbout@physchem.uni-wuppertal.de. Permanent address: Institute of Chemical Physics, Russian Academy of Sciences, 117334 Moscow, Russian Federation.

‡ Kansas State University. E-mail: setserdw@ksu.edu.

10.1021/jp001705q CCC: $19.00
Published on Web 09/28/2000

TABLE 1: Thermodynamic and Kinetic Data for Primary and Secondary Reactions

reaction	k(298 K)/ cm^3 molecule^{-1} s^{-1}	E_a/ kcal mol^{-1}	ref	$-\Delta H_0°$/ kcal mol^{-1}	$\langle E_{av}\rangle$
(1) OH + $CH_3C(O)H$ → H_2O + CH_3CO	$(1.4 \pm 0.2) \times 10^{-11}$	-0.5 ± 0.2	8	30.2	32.6
(2) OD + $CH_3C(O)$ → HOD + CH_3CO				30.5	32.9
(3) NO_2 + CH_3CO → $CH_3C(O)ONO$	$(2.5 \pm 0.6) \times 10^{-11}$	<1	9		
(a) → CH_3CO_2 + NO				33.5	
(b) → CH_3 + CO_2 + NO				43.0	
(4) OH + CH_3CO → $CH_3C(O)OH$	7×10^{-11}		10		
(a) → H_2O + CH_2CO				76.2	
(b) → CH_4 + CO_2				118.9	
(5) NO + CH_3CO → $CH_3C(O)NO$					
(a) → $CH_3C(O)NO$	$(2.4 \pm 0.1) \times 10^{-11}$		11		
(b) → CH_2CO + HNO				7.4	
(8) H + CH_3CO → products	5.5×10^{-11}		12		
(a) → H_2 + CH_2CO	35%		13	62.1	
(b) → CH_3 + HCO	85% (65%)		12(13)	4.1	
(c) → CH_4 + CO	<6%			93.9	
(d) → $CH_3C(O)H$	10%		12		

recorded by a Fourier transform infrared spectrometer (BIO-RAD) from a fast-flow reactor at 298 K. The spectral resolution was 1 cm^{-1}. The response of the liquid N_2 cooled InSb detector was calibrated with a standard blackbody source. Ar was used as the carrier gas, and the total pressure in the 4 cm diameter reactor was 0.5−2.0 Torr depending on the degree of throttling of the flow; the corresponding reaction times were $\Delta t = 0.22-0.9$ ms. Ar, H_2, or D_2, and NO_2 were metered to the reactor using standard methods. Commercial tank grade Ar was passed in succession through three molecular sieve traps cooled by either an acetone/dry ice mixture or liquid nitrogen to remove impurities. Tank grade H_2 was used without purification.

The OH (or OD) radicals were produced 30 cm upstream of the observation window (NaCl) via the fast H(D) + NO_2 → OH(OD) + NO reaction, which also was the source of NO molecules. The H atoms were generated by a microwave discharge in a $H_2(D_2)$/Ar mixture; the degree of the dissociation was 50% as determined by ArH* emission.[15] During the study of the primary reaction, the initial concentration of H atoms was in the range of $(1-2) \times 10^{12}$ molecules cm^{-3}. Acetaldehyde (Fisher Scientific) was introduced into the reactor through the injector located 3.5 cm upstream of the observation window. Typical CH_3CHO concentrations were about 3×10^{13} molecules cm^{-3}. The typical concentration of NO_2 for study of the primary and NO_2 + HCO secondary reactions was about 1×10^{14} molecules cm^{-3}. The best conditions to observe the secondary reactions of OH and NO were $[NO_2] \approx [H_2] \approx 3 \times 10^{13}$ molecules cm^{-3}. To favor the H + CH_3CHO secondary reaction, an excess of H atom concentration was needed, for which the initial hydrogen concentration was elevated up to $[H_2] \approx 8 \times 10^{13}$ molecules cm^{-3}.

2.2. Spectral Simulation. The simulation procedure using the least-squares method to match the computed water spectra with the experimental ones has been described in full.[2,3] The obtained vibrational distributions are for collisionally equilibrated reservoirs of the resonant modes, namely, the ν_1 and ν_3 modes of H_2O, and the ν_1 and $2\nu_2$ modes of HDO. Accordingly, quantum numbers $\upsilon_{1,3} = \upsilon_1 + \upsilon_3$ and $\upsilon_{1,2} = \max \upsilon_2$ ($i = 0$ in the group of equilibrated levels $(\upsilon_1, \upsilon_2, \upsilon_3)/(\upsilon_1 + i, \upsilon_2 - 2i, \upsilon_3)$, $i = 0, 1, ...$) are used to describe vibrational distributions of H_2O and HOD, respectively. The uncertainties of the vibrational populations obtained from the simulation methods were analyzed previously.[2,4] Usually, the ratio of populations in stretching states υ_3 (or $\upsilon_{1,3}$ in the case of H_2O) = 1 and 2, $P_\upsilon(1)/P_\upsilon(2)$, can be determined with an accuracy better than 10%. The main error in determining the total vibrational energy results from an uncertainty in estimation of populations in the nonemitting ("dark") states, namely, $(0\upsilon_20)$ states of H_2O and (000) and (010) states of HOD. Estimations with the help of surprisal plots (information theory) give uncertainties in $P(0)$ in the range of 10−30% depending on the signal-to-noise ratio. The emission from the OH(OD) + $CH_3C(O)H$ reactions was relatively strong, and short reaction times, $\Delta t \approx 0.2$ ms, could be employed for the primary reaction. Except for the equilibration of the resonant levels, vibrational relaxation of H_2O and HOD should be minimal.[2,3] Comparison of H_2O spectra measured at different reactor pressures showed that vibrational relaxation was not important for pressure ≤0.7 Torr.[3]

The CO_2 simulation procedure has been fully described elsewhere.[16] The observed emission is calculated as a superposition of $\Delta\upsilon_3 = -1$ transitions from $(\upsilon_1, \upsilon_2^l, \upsilon_3)-(\upsilon_1, \upsilon_2^l, \upsilon_3 - 1)$ combination bands with rigid-rotor approximation for vibrational−rotational line intensities. The simulation cannot distinguish between transitions from $\upsilon_3 = 1$ and $\upsilon_3 > 1$ states because of the overlap of the $(\upsilon_1, \upsilon_2, \upsilon_3)$ and $(\upsilon_1, \upsilon_2 - 2, \upsilon_3 + 1)$ bands. Calculations were made for the $\upsilon_3 = 1$ state with bending excitation, and the actual υ_3 distribution may be somewhat broader. Comparison of carbon dioxide spectra measured at different pressures proved that vibrational relaxation was not important in experiments with $P < 1.0$ Torr ($\Delta t < 0.5$ ms).[16] Assignment of the vibrational distribution of CO was carried out as in ref 7.

3. Results

3.1. Chemical Reactions in the H/NO_2 + $CH_3C(O)H$ System. Raw emission spectra from the H/NO_2 + $CH_3C(O)H$ chemical system are shown in Figure 1. The spectra measured at a total pressure of 1 Torr ($\Delta t = 0.45$ ms) correspond to different relations between the initial NO_2 and H_2 concentrations in the reactor. The spectra, which are normalized to the maximum intensity, represent an average of 1024 scans of the spectrometer. All the spectra contain H_2O emission in the 3200−3900 cm^{-1} range from the primary reaction 1. This emission consists mainly of $\Delta\upsilon_3 = -1$ transitions (asymmetric stretch). In addition to H_2O emission, the spectra displayed intense chemiluminescence in the 2000−2800 cm^{-1} range, which was attributed to the secondary reactions of acetyl radical with NO_2, NO, OH, and H. The dominant secondary reaction depends on the relative concentrations of the reactants, and we can distinguish three cases.

A. $[NO_2] \gg [H_2]$ (Figure 1a). In a large excess of NO_2 the only important secondary reaction is reaction 3

$$NO_2 + CH_3CO \rightarrow CH_3C(O)ONO \rightarrow CH_3 + CO_2 + NO \quad (3)$$

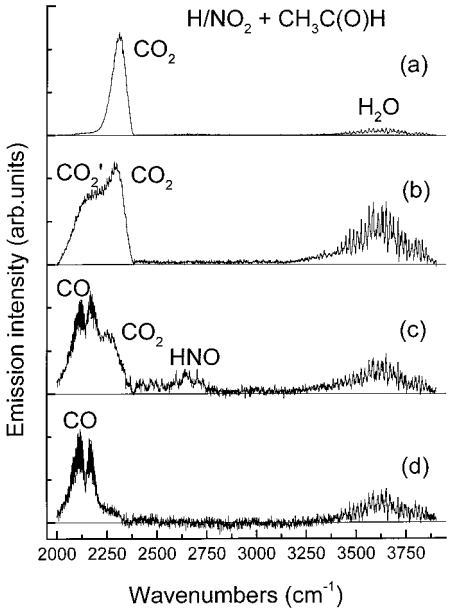

Figure 1. Raw infrared emission spectra from the $H/NO_2 + CH_3C(O)H$ chemical system: (a) at 1 Torr ($\Delta t = 0.5$ ms), $[NO_2] = 2 \times 10^{14}$ molecules cm^{-3}, and $[H_2] = 7 \times 10^{12}$ molecules cm^{-3}; (b) at 0.8 Torr ($\Delta t = 0.4$ ms), $[NO_2] = 1 \times 10^{14}$ molecules cm^{-3}, and $[H_2] = 2.5 \times 10^{13}$ molecules cm^{-3}; (c) at 2 Torr ($\Delta t = 1$ ms), $[NO_2] = 1 \times 10^{14}$ molecules cm^{-3}, and $[H_2] = 8 \times 10^{13}$ molecules cm^{-3}; (d) at 1.2 Torr ($\Delta t = 0.6$ ms), $[NO_2] = 2.3 \times 10^{13}$ molecules cm^{-3}, and $[H_2] = 5.3 \times 10^{13}$ molecules cm^{-3}. The spectra are normalized to the maximum peak intensity.

with an overall rate constant $k_3 = 2.5 \times 10^{-11}$ cm^3 $molecule^{-1}$ s^{-1}.[9] Figure 1a corresponds to $[NO_2] = 2 \times 10^{14}$ molecules cm^{-3} and $[H_2] = 7 \times 10^{12}$ molecules cm^{-3}, which provides the highest $[NO_2]/[H_2] \cong 30$ ratio used in the experiments. The observed products are H_2O from the primary reaction and CO_2 in the 2200−2400 cm^{-1} range. This observation agrees with the results of Slagle and Gutman,[9] who found reaction 3 to be the dominant reaction.

B. $[H_2] \approx [NO_2]$. If the NO_2 concentration is reduced relative to H_2, $[NO_2] = 1.0 \times 10^{14}$ molecules cm^{-3} and $[H_2] = 2.5 \times 10^{13}$ molecule cm^{-3}, higher CO_2 excitation becomes observable as emission extends to the 2000−2200 cm^{-1} range (Figure 1b). This emission closely resembles the CO_2 chemiluminescence from decomposition of chemically activated acetic acid[16] and can be assigned to the fast secondary reaction of acetyl radicals with OH radicals (reaction 4)

$$OH + CH_3CO \rightarrow CH_3C(O)OH \rightarrow H_2O + CH_2CO \quad (4a)$$

$$\rightarrow CH_4 + CO_2 \quad (4b)$$

with the overall rate constant $k_4 = 7 \times 10^{-11}$ cm^3 $molecule^{-1}$ s^{-1}.[10] The branching ratio of dehydration to decarboxylation channels was estimated in our study of unimolecular decomposition of chemically activated acetic acid as 2:1 in favor of the dehydration channel a.[16] This result was confirmed by theoretical work.[17] It is necessary to mention that the water-forming channel (reaction 4a), which was found to be a dominant pathway of reaction 4, is ~76 kcal mol^{-1} exothermic (see Table 1), and, hence, produces vibrationally excited H_2O. The vibrational distribution for this excitation was determined[16] as $P(0-3) = 54$, 35, 9, and 2. Consequently, precautions must be taken to avoid contribution of $v_{1,3} = 1 \rightarrow 0$ and $2 \rightarrow 1$ emission from reaction 4 during the study of the primary reaction 1. Figure 1b reflects the competition between reactions 3 and 4, since CO_2 emission from both reactions 3a and 4b is observed.

If the NO_2 and H concentrations are comparable, $[NO_2] = 1 \times 10^{14}$ molecules cm^{-3} and $[H_2] = 8 \times 10^{13}$ molecules cm^{-3}, CO and HNO emission in the 2000−2800 cm^{-1} range becomes observable (Figure 1c). The 2300−2800 cm^{-1} emission is characteristic for the $\Delta v_1 = -1$ transitions from the HNO molecule studied earlier.[18] This product can be explained by the secondary reaction of NO with HCO (reaction 6) rather than by reaction 5b.

$$NO + CH_3CO \rightarrow CH_3CONO \quad (5a)$$

$$\rightarrow HNO + CH_2CO \quad (5b)$$

$$NO + HCO \rightarrow HNO + CO \quad (6)$$

The HCO radicals can be formed due to the incomplete conversion of H atoms to OH radicals at high hydrogen concentrations (see reaction 8a). Reaction 5b can be eliminated from consideration of thermochemistry, since the $\Delta H_f°$ values of NO, CH_3CO, CH_2CO, and HNO, which are 21.7, −0.9, −10.6, and 23.8 kcal mol^{-1}, respectively, give the enthalpy of reaction 5b as -7.4 ± 1.0 kcal mol^{-1}. This energy is insufficient for the excitation of the observed ν_1(H−NO) stretching mode of HNO, and formation of HNO must be explained by the occurrence of reaction 6. The rate constant for reaction 5a was measured to be $k_5 = (2.4 \pm 0.7) \times 10^{-11}$ cm^3 $molecule^{-1}$ s^{-1} at 1 atm of pressure.[11] This value is a high-pressure limit consistent with the known rate coefficients for the combination reactions of NO with other alkyls, i.e., $k(NO + CH_3COCH_2) = (2.6 \pm 0.3) \times 10^{-11}$ cm^3 $molecule^{-1}$ s^{-1}, and formyl radical, $k(NO + HCO) = (1.2 \pm 0.1) \times 10^{-11}$ cm^3 $molecule^{-1}$ s^{-1}. We cannot exclude the possibility that at low pressure CH_3CONO can partly decompose to give CH_2CO and HNO products without significant vibrational excitation. The CO signal in the 2000−2200 cm^{-1} range also can be a result of the tertiary reaction of HCO radicals with either NO or OH:[7]

$$OH + HCO \rightarrow HOC(O)H \rightarrow H_2O + CO \quad (7)$$

C. $[H_2] \gg [NO_2]$. In an excess of hydrogen, the important reactions are the primary reaction 1 and reaction 8

$$H + CH_3CO \rightarrow CH_3C(O)H \rightarrow CH_3 + HCO \quad (8a)$$

$$\rightarrow H_2 + CH_2CO \quad (8b)$$

$$\rightarrow CH_4 + CO \quad (8c)$$

$$\rightarrow CH_3C(O)H \quad (8d)$$

with $k_8 = 5.5 \times 10^{-11}$ cm^3 $molecule^{-1}$ s^{-1}.[12] The reaction of hydrogen atoms with acetaldehyde, $H + CH_3C(O)H \rightarrow CH_3CO + H_2$, with the rate coefficient $k \cong 8 \times 10^{-14}$ cm^3 $molecule^{-1}$ s^{-1} [13,19] is too slow to play any role in our experiments. The only products observable by IRCL are the primary product water and CO. As can be seen from Figure 1d, the experiment with $[NO_2] = 2.3 \times 10^{13}$ molecules cm^{-3} and $[H_2] = 5.3 \times 10^{13}$ molecules cm^{-3} does give a strong CO emission. This observation can be explained by the occurrence of reaction 8c or by the tertiary reaction 9.

$$H + HCO \rightarrow H_2 + CO \quad (9)$$

The obtained vibrational distribution of CO was $P_v = 100$, 25, 12, and ~5 for $v = 1$, 2, 3, and 4, respectively. This distribution is similar to P_v(CO) from reaction 9.[7] The mechanism of reaction 8 at low pressure and 298 K was determined by the discharge flow technique combined with mass-spectrometric detection

TABLE 2: Vibrational Distribution of H_2O from the Reaction of OH with $CH_3C(O)H$

$\upsilon_{1,3}$[a]	$\upsilon_2 = 0$	$\upsilon_2 = 1$	$\upsilon_2 = 2$	$\upsilon_2 = 3$	$\upsilon_2 = 4$	$\upsilon_2 \geq 5$	$P_{1,3}$[b]	$P_{1,3}$[c]	$P_{1,3}°$
0	5.7	5.9	4.9	3.5	1.7	1.3	−	23.0	55.1
1	12.9	13.4	11.2	8.1			59.2	45.6	34.9
2	19.3	9.9					38.0	29.2	9.84
3	2.2						2.8	2.2	0.22
P_2[d]	40.1	29.2	16.1	11.6	1.7	1.3			
$P_2°$	43.1	26.2	15.6	8.4	4.2	2.5			

[a] $\upsilon_{1,3} = \upsilon_1 + \upsilon_3$. [b] $P_{1,3}(0)$ is neglected. [c] $P_{1,3}(0)$ from the linear surprisal plot. [d] See the text for the assignment of the bending distribution in $\upsilon_{1,3} = 0$. $P^0_{1,3}$ is the statistical distribution.

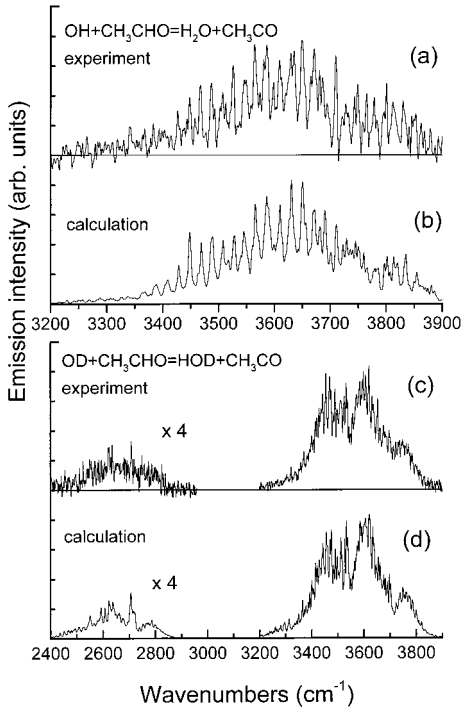

Figure 2. (a) Simulation of the H_2O spectrum from the OH + $CH_3C(O)H$ reaction. (b) Simulation of the HOD spectrum from the OD + $CH_3C(O)H$ reaction. The spectra were measured at 0.5 Torr ($\Delta t = 0.25$ ms), $[NO_2] = 1.7 \times 10^{14}$ molecules cm^{-3}, $[H_2]$ or $[D_2] = 2 \times 10^{13}$ molecules cm^{-3}, and $[CH_3CHO] = 1 \times 10^{13}$ molecules cm^{-3}. The calculated spectra correspond to the vibrational distributions in Tables 2 and 3.

using resonance-enhanced multiphoton ionization[12] and electron-impact ionization.[13] In both studies channel 8a was found to be the main route, with branching fractions of 85 ± 20%[12] and 65 ± 4%.[13] The branching factor for channel 8b was determined to be 35 ± 2%,[13] and that of the stabilization channel 8d at a pressure of 0.7 Torr was determined to be on the order of 10 ± 5%.[12] From these data, channel 8c can be estimated as minor (<6%) and our observation of CO in an excess of hydrogen should result from successive reactions 8a and 9.

3.2. H_2O and HOD Vibrational Distributions from the Primary OH(OD) + $CH_3C(O)H$ Reaction. Since reaction 3 does not produce water, conditions with a short reaction time, $\Delta t = 0.25$ ms, and $[NO_2] \gg [H_2]$ were used to obtain spectra from which the nascent H_2O and HOD distributions from reaction 1 were obtained. Figure 2a shows the H_2O spectrum measured at 0.5 Torr with $[NO_2] = 1.7 \times 10^{14}$ molecules cm^{-3} and $[H_2] = 2 \times 10^{13}$ molecules cm^{-3} and corrected for the response function. Panel b of Figure 2 presents the best calculated spectrum. The distribution presented in Table 2 is the average from fitting four spectra measured at conditions similar to those of Figure 2. The stretching H_2O distribution $P_{1,3}(\upsilon_{1,3})$ in Table 2 is the summation over the bending quantum number υ_2. The distribution $P_{1,3}(\upsilon_{1,3}) = 59{:}38{:}3$ for $\upsilon_{1,3} = 1$, 2, and 3 states extends to the energy limit $\upsilon_{1,3} = 3$ and decreases with increasing $\upsilon_{1,3}$. A population in $\upsilon_{1,3} = 0$, $P_{1,3}(0) = 23.0 \pm 3.8$ for the average renormalized full distribution, was determined with the help of a linear surprisal analysis described below. The full distribution given in the column $P_{1,3}$[c] has the maximum population, ~45%, in $\upsilon_{1,3} = 1$. The global bending distribution for $\upsilon_{1,3} = 1$, 2, and 3 states decreases with υ_2, although the bending distribution for the $\upsilon_{1,3} = 1$ stretching state has a maximum in $\upsilon_2 = 1$.

Full HOD spectra, including the $\Delta\upsilon_2 = -2 + \Delta\upsilon_1 = -1$ emission in the 2400−3000 cm^{-1} region, were measured at conditions similar to those described above for H_2O. Figure 2c shows the $\Delta\upsilon_3 = -1$ and $\Delta\upsilon_2 = -2 + \Delta\upsilon_1 = -1$ HDO spectra measured at 0.5 Torr, $[NO_2] = 1.7 \times 10^{14}$ molecules cm^{-3} and $[D_2] = 2.1 \times 10^{13}$ molecules cm^{-3}, and the calculated spectrum according to the distribution given in Table 3 is presented in Figure 2d. The obtained $P_3(0-3) = 25{:}39{:}33{:}2$ distribution, giving populations in υ_3, shows an inverted distribution for the newly formed O−H bond with nearly equally populated $\upsilon_3 = 1$ and $\upsilon_3 = 2$ states. Populations in the "dark" (000) and (010) states were assigned as equal to the populations in the (020)/(100) and (030)/(110) diads, respectively, which is rather close to statistical distribution. The uncertainty of this assignment can be taken as half of the population in the dark state, and the resulting $P_3(0)$ can be expressed as 25.2 ± 3.7. This value agrees with the $P_{1,3}(0)$ value for H_2O, confirming the validity of the surprisal extrapolation for H_2O. The difference in the $P_{1,3}(H_2O)$ and P_3(HOD) distributions will become clearer after the analysis below.

The theoretical-information analysis of the vibrational distributions for H_2O and HDO from reactions 1 and 2 was carried out using the methods described in our previous papers.[2,3] Prior distributions were calculated assuming the same rate of formation of all the internal quantum states of products at a given total energy (we may also call them "statistical" distributions). Direct summation over the H_2O and HOD rotational states was carried out. The prior distributions, $P_{1,3}°$ and $P_3°$, were calculated for the model in which a radical fragment R is treated as an atom (model I). From our previous studies, we know that the internal degrees of freedom of R usually are not involved in the energy disposal for direct H atom abstraction. Tables 2 and 3 contain prior distributions for this model, and Figure 3 presents the corresponding surprisal plots for HOD (a) and H_2O (b). In calculations of the surprisals presented in Figure 3, the experimental distributions $P_{1,3}$ and P_3 obtained by averaging four H_2O and four HDO simulations, respectively, were used.

The HOD surprisal plot in Figure 3a, which is $-\ln(P_3/P_3°)$ vs $\langle f_{\upsilon_3}\rangle = \langle E_{\upsilon_3}\rangle / \langle E_{av}\rangle$, directly reflects the deviation of the excitation of the newly formed H−OD bond from the statistical expectation. The surprisal plot of the OD + CH_3CHO reaction is linear, with a slope of $-\lambda_{\upsilon_3} = 4.9 \pm 0.4$, and has an intercept with the ordinate axis, $f_{\upsilon_3} = 0$, of $\lambda_3° = -0.99 \pm 0.22$, giving

TABLE 3: Vibrational Distribution of HDO from the Reaction of OD with $CH_3C(O)H$

v_3	$v_{1,2}{}^a = 0$	$v_{1,2}{}^a = 1$	$v_{1,2}{}^a = 2$	$v_{1,2}{}^a = 3$	$v_{1,2}{}^a = 4$	$v_{1,2}{}^a = 5$	$v_{1,2}{}^a \geq 6$	P_3	$P_3{}^b$	$P_3{}^\circ$
0	4.0[c]	3.4[c]	4.0	3.4	3.7	3.6	3.1	25.2	27.5	76.5
1	14.1	5.9	10.7	2.7	2.6	3.1		39.1	37.9	20.3
2	19.9	10.2	2.4	0.9				33.4	32.3	3.1
3	1.7	0.7						2.4	2.3	0.08
$P_{1,2}$	39.7	20.2	17.1	7.0	6.3	6.7	3.1			
$P_{1,2}{}^\circ$	21.2	15.2	21.1	14.0	13.1	7.4	7.8			

[a] See section 2.2 for the definition of $v_{1,2}$. [b] $P_3(0)$ from the linear surprisal plot. [c] Populations in the dark (000) and (010) states were assumed to be equal to the populations in the collisionally coupled (020/100) and (030/110) pairs of states, respectively; $P_3^0$is the statistical distribution.

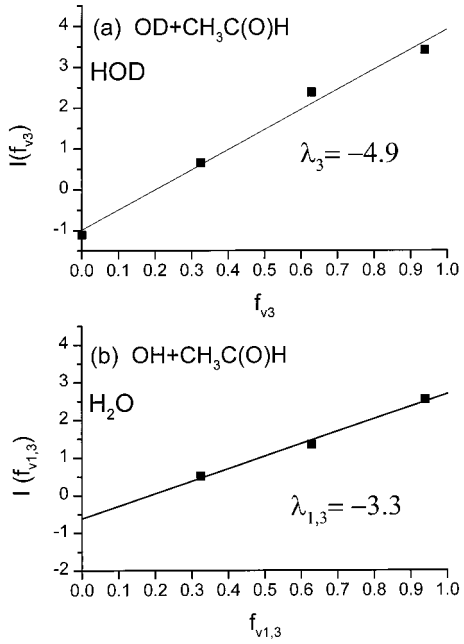

Figure 3. Vibrational surprisal plots for the stretching distributions of (a) HOD from the OD + CH_3CHO reaction and (b) H_2O from the OH + CH_3CHO reaction.

$P_3(0) = 27.5 \pm 4.4$ in the renormalized total population $P_3(0{:}1{:}2{:}3) = 28{:}38{:}32{:}2$. Taking into account the uncertainty given by the standard deviation of the surprisal plot, this value is in good agreement with the $P_3(0) = 25 \pm 4$ obtained from the spectral simulation. The H_2O surprisal plot, $-\ln(P_{1,3}/P_{1,3}{}^\circ)$ vs $\langle f_{v_{1,3}}\rangle = \langle E_{v_{1,3}}\rangle/\langle E_{av}\rangle$, is presented in Figure 3b and shows less decline, since the vibrational populations and corresponding surprisals are related to the mixture of the "active" and "spectator" local O−H mode vibrations, which are observed as a mixture of ν_1 and ν_3 normal modes. For the distribution from reaction 1 the slope is $-\lambda_{v_{1,3}} = 3.3 \pm 0.3$. The intercept with the $f_{v_{1,3}} = 0$ axis is $\lambda_{1,3}{}^\circ = -0.61 \pm 0.22$, giving the renormalized full population $P_{1,3}(0{:}1{:}2{:}3) = (23 \pm 4){:}46{:}29{:}2$. In calculation of the total vibrational energy, the bending distribution in $v_{1,3} = 0$ was estimated assuming a similarity with $v_{1,3} = 1$ for $v_2 = 0-3$, while higher bending populations were assigned using a geometric progression decreasing by a factor of 0.5 for energetically allowed (040)−(060) states. Having the total vibrational distribution, the fraction of energy released as the vibrational energy of H_2O was found to be $\langle f_v\rangle = 0.51 \pm 0.03$. The fraction released to bending excitation is $\langle E_{2v}\rangle/\langle E_v\rangle = 0.30$. For the isotopic reaction 2, $\langle f_v\rangle = 0.53 \pm 0.02$ and the fraction released to the O−H vibration stretch mode is $\langle E_{3v}\rangle/\langle E_v\rangle = 0.65$ for $P_3(0) = 25\%$ from the simulations. The energy disposal data along with the results for several other hydroxyl reactions are summarized in Table 4.

3.3. CO_2 Excitation from NO_2 and OH Reactions with CH_3CO. The spectrum of CO_2 from reaction 3 recorded at 0.8 Torr, $[NO_2] = 2.4 \times 10^{14}$ molecules cm^{-3}, and $[H_2] = 1.5 \times 10^{13}$ molecules cm^{-3} and corrected for the response function is shown in Figure 4a. It features a broad structure between 2200 and 2400 cm^{-1} with Q-branch peaks belonging to different v_2's of the $v_3 = 1 \rightarrow v_3 = 0$ transition. The simulated spectrum is presented below. The diagram in Figure 5 shows the CO_2 "bending" distribution $P_{1,2}(v_2)$ averaged over the three measured spectra. We have to use quotation marks because $2\nu_2$ (1285 cm^{-1}) and ν_1 (1388 cm^{-1}) modes are collisionally coupled, and notions v_2 and $P_{1,2}$ have the same meaning as in the case of HOD. The symmetric stretching excitation in CO_2 is not expected to be excited, and the observed excitation is presumably initially produced in the bending vibrations. This experimental $P_{1,2}$ distribution assumes that a complete equilibration between the resonant $2\nu_2$ and ν_1 levels takes place. All three spectra showed the maximum population in $v_2 = 1$ with levels populated up to $v_2 = 10$.

The CO_2 chemiluminescence from the OH + CH_3CO reaction is shown in Figure 4b. It is a difference spectrum obtained after subtraction of the contribution from reaction 3 from a spectrum such as shown in Figure 1b. Although some uncertainty exists in the intensity of the emission from the $v_2 = 1-5$ levels, simulation of the difference spectrum gives the bending $P_{1,2}(v_2)$ distribution extended up to $v_2 = 25$ with a maximum population in $v_2 = 8$ (Figure 5). As expected, this distribution is similar to that obtained for the unimolecular decomposition of chemically activated acetic acid with an excitation energy of 95.3 kcal mol^{-1}, which has been isolated and studied in our apparatus.[16] In that study both dissociation channels

$$CH_3C(O)OH^* \rightarrow H_2O + CH_2CO \qquad (10a)$$

$$\rightarrow CH_4 + CO_2 \qquad (10b)$$

were observed by the IR emission of H_2O and CO_2 products, and the highest observed CO_2 bending state was $v_2 = 24$ with peak population on $v_2 = 8-9$.

4. Discussion

4.1. Primary OH(OD) + $CH_3C(O)H$ Reaction. Comparison of energy disposal in Table 4 shows that the mean fraction of available energy released as vibrational energy to H_2O and HOD in reactions 1 and 2 is close to $\langle f_v\rangle$ for the reactions with CH_2O and $(CH_3)_2S$ and lower than $\langle f_v\rangle$ for reactions with *n*-butane and cyclohexane. The latter proceed by abstraction of the secondary H atoms from the alkanes. The stretching distribution is inverted and peaked on $v_3 = 1$ (and $v_{1,3} = 1$). Actually, the $P_3(v_3)$ distribution is more indicative of the character of the reaction, as $P_{1,3}(v_{1,3})$ can happen to be "inverted", with both $P_1(v_1)$ and $P_3(v_3)$ decreasing. A better characterization is the deviation from the prior distribution expressed via the slope of the surprisal plot. We can see from Table 4 that λ_{v_n} values for acetaldehyde reaction are close to that for formaldehyde and dimethyl sulfide,

TABLE 4: Summary of Energy Disposal

reaction	$\langle E_{av}\rangle^a$	$-\lambda_{v_n}$	$\langle f_v\rangle$	$\langle E_{v_3}\rangle/\langle E_v\rangle^b$	ref
$OH + CH_3C(O)H \rightarrow H_2O + CH_3CO$	32.6	3.3	0.51	0.30	this work
$OH + CH_2O \rightarrow H_2O + HCO$	32.9	3.2	0.56	0.34	7
$OH + DMS \rightarrow H_2O + CH_3SCH_2$	27.5	3.2	0.53	0.30	4
$OH + C_6H_{12} \rightarrow H_2O + C_6H_{11}$	27.1	5.7	0.62	0.14	1
$OH + C_4H_{10} \rightarrow H_2O + C_4H_9$	24.7	5.5	0.65	0.19	1
$OD + CH_3C(O)H \rightarrow HDO + CH_3CO$	32.8	4.9	0.53	0.65	this work
$OD + CH_2O \rightarrow HDO + HCO$	33.2	5.1	0.54	0.63	7
$OD + DMS \rightarrow HDO + CH_3SCH_2$	27.8	4.9	0.55	0.64	4
$OD + C_6H_{12} \rightarrow HDO + C_6H_{11}$	27.4	6.3	0.56	0.82	1
$OD + C_4H_{10} \rightarrow HDO + C_4H_9$	25.0	6.3	0.59	0.79	1

[a] In kcal mol^{-1}. Available energies for deutero-isotopic reactions were calculated accounting for a change in zero vibration energies. [b] The fraction of the total vibrational H_2O energy released to the bending mode, $\langle E_{v_2}\rangle/\langle E_v\rangle$, in reactions with OH and the fraction of HOD vibrational energy found in the O−H mode, $\langle E_{v_3}\rangle/\langle E_v\rangle$, for reactions with OD.

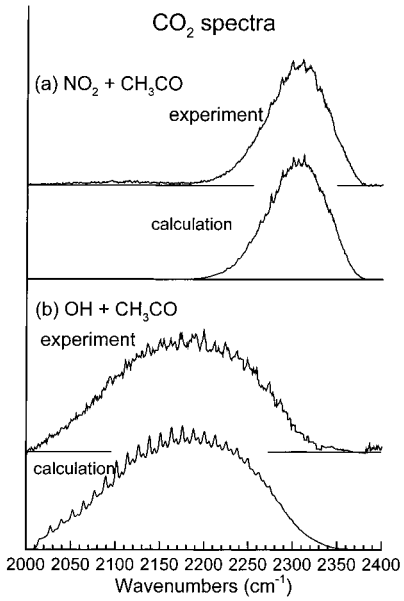

Figure 4. Comparison of the experimental (upper curves) and simulated (lower curves) CO_2 spectra: (a) from the $NO_2 + CH_3CO$ reaction with $[NO_2] = 2.4 \times 10^{14}$ molecules cm^{-3}, $[H_2] = 1.5 \times 10^{13}$ molecules cm^{-3}, and $\Delta t = 0.25$ ms; (b) from the $OH + CH_3CO$ reaction with $[NO_2] = 7.2 \times 10^{13}$ molecules cm^{-3}, $[H_2] = 2.5 \times 10^{13}$ molecules cm^{-3}, and $\Delta t = 0.25$ ms.

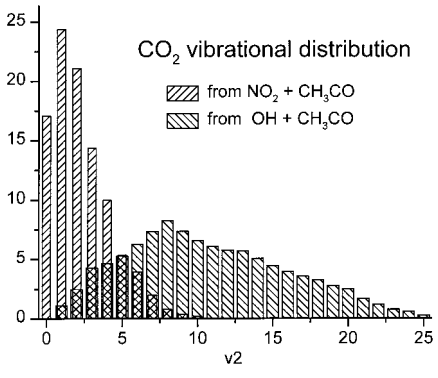

Figure 5. Vibrational (bending) distribution of CO_2 from the $NO_2 + CH_3CO$ and $OH + CH_3CO$ reactions.

but substantially less than the corresponding values for hydrocarbon reactions (all values are for the model I prior calculation). A slight trend for less energy in the bending vibration compared to the $OH + CH_2O$ reaction can be noted. The difference with hydrocarbons is even more evident if we consider partitioning of the vibrational energy between different vibrational modes. The fraction of vibrational energy in bending, $\langle E_{v_2}\rangle/\langle E_v\rangle$, is equal to 0.30 for reaction 1 and less than 0.20 in the case of hydrocarbons. On the other hand, the energy in the newly formed O−H bond determined from reaction 2, $\langle E_{v_3}\rangle/\langle E_v\rangle$, is 0.65 compared to ∼0.80 for hydrocarbons. It can be concluded that, compared with that of hydrocarbons, reaction with the C−H bond of aldehydes disposes more energy to bending vibrations at the expense of less excitation of the new O−H bond. Accordingly, in the OH + aldehyde reactions, the H atom of the initially existing O−H bond cannot be regarded as a complete spectator.

Reaction 1 has been studied using ab initio calculations at the MP3[21] and VMP2/6-311G**[22] levels of theory. The optimized transition state (TS) HO−H′−C(O)CH_3 geometry corresponds to R(O−H) = 0.967 Å, R(O−H′) = 1.395 Å (+43.8%), R(C−H′) = 1.180 Å (+6.7%), ∠O−H′−C = 168.4°, and ∠H−O−H = 94.5° (−9.6%). Figures in parentheses show the deviation from the equilibrium parameters in H_2O or CH_3C(O)H molecules. The structure of the TS is more reactant-like in character and shows a strong H′ vector in the direction of the O atom. This TS resembles the TS's for H atom abstraction from CH_2O[23] and $(CH_3)_2S$[24], as well as from alkanes (for example, the variational TS theory calculation for the OH + C_3H_8 reaction):[25] they all show nearly collinear H′ atom transfer and an H−O−H′ angle close to the equilibrium angle in the water molecule. An important difference between OH reactions with aldehydes and *n*-butane on cyclohexane is that the former are barrierless and exhibit a negative activation energy, while the latter have $E_a \cong 0.8$ kcal mol^{-1}. In both cases, the energy disposal corresponds to the release of energy after passing the critical configuration. The larger bending-to-stretching excitation ratio for aldehydes can have (at least) two explanations: (i) the entrance channel for aldehydes has fewer restrictions with regard to the HO−H′−C bending angle, and angles differing from ∼109° permit larger bending excitation; (ii) the exit channel potential energy surface for aldehydes induces coupling between the stretching and bending modes of water as the potential energy is released and as the two products separate. For whatever reason, a correlation seems to exist between reduced $\langle E_{v_2}\rangle/\langle E_v\rangle$ and a smaller reaction rate constant per available H atom. Formation of the bound complex in the exit channel could explain some decrease of energy in the stretching vibrations, but nevertheless, the obtained $\langle f_v\rangle \cong 0.52$ and $-\lambda_{v_3} = 4.9$ are typical for direct abstraction reactions with an early transition state.

4.2. Secondary NO_2, OH, and H + CH_3CO Reactions. The $NO_2 + CH_3CO$ (3) reaction was studied by Slagle and Gutman[9] using the infrared multiphoton-induced decomposition of CF_2Cl_2 to produce Cl atoms, which reacted with acetaldehyde, giving CH_3CO radicals. The acetyl radicals and other reaction products were monitored by time-resolved photoionization mass spectrometry. From observation of the NO and CH_3 radicals

and the absence of other products, the authors concluded that the reaction proceeds mainly by formation of methyl radicals. The shape of the temporal profiles of the CH_3^+ ion signal could be simulated by a mechanism in which the acetoxy radicals CH_3CO_2, produced from decomposition of the $CH_3C(O)ONO$ complex, rapidly decomposed to give $CH_3 + CO_2$. This is in accord with the $D_{298}(CH_3{-}CO_2) = -10$ kcal mol^{-1} estimated from the heats of formation of CH_3CO_2, CO_2, and CH_3.[8] Our direct observation of CO_2 confirms these results, and the observed bending excitation corresponds to the evolution from the bent O−C−O configuration in the intermediate CH_3CO_2 radical to linear CO_2 geometry. At the same time, the lifetime of the initially formed $CH_3C(O)ONO$ adduct should be sufficient to allow redistribution of energy to the methyl group. The CO_2 distribution from reaction 3 is peaked at $v_2 = 1$ and the highest observed $v_2 = 10$ (see Figure 5). This distribution is a little colder than that from the $NO_2 + HCO$ reaction, which has a maximum on $v_2 = 2$ and extends to $v_2 = 13$.[7] However, the available energy in reaction 3 is about 3 kcal mol^{-1} larger than in $NO_2 + HCO \rightarrow H + CO_2 + NO$ reaction. This can be an indication that the methyl group takes part in the reaction dynamics and that the reaction indeed proceeds through formation of acetoxy radicals. It is important to note that the $F + HC(O)OH$ reaction does not give CO_2 emission in the 2000−2400 cm^{-1} range, which is the most sensitive region for the InSb detector.[26] Even though HCO_2 is not a stable radical, the extra energy from the decomposition of RC(O)O−NO is critical for the excitation of the asymmetric stretching mode of CO_2.

The interesting difference between the reactions of NO_2 with formyl and acetyl radicals is that two different intermediate adducts can lead to two sets of products: $HC(O)NO_2$ gives $HONO + CO$, and $HC(O)ONO$ gives $(H + CO_2) + NO$. Both CO and CO_2 were observed in our previous IRCL study.[7] In the acetyl reaction, the $CH_3C(O)NO_2$ complex can also be initially formed, which can be followed by redissociation, collisional stabilization, or elimination of CH_3ONO or HONO. The $NO_2 + CH_3CO \rightarrow CH_3ONO + CO$ and $CH_2CO + HONO$ reaction channels are exothermic by 48 and 36 kcal mol^{-1}, respectively. Nevertheless, unlike the four-centered migration of the H atom in the $HC(O)NO_2$ intermediate, giving $HONO + CO$, no products indicating formation of the $CH_3C(O)NO_2$ intermediate were observed in our study or in the study of Slagle and Gutman.[9] In the latter work the authors failed to detect $CH_3C(O)NO_2$, CH_2CO, or HNO_2 at 1−2 Torr in their experiments. Hence, the probable fate for $CH_3C(O)NO_2$ is redissociation or isomerization to $CH_3C(O)ONO$.

The most important question for the $OH + CH_3CO$ reaction is whether it proceeds via addition/elimination or by a direct abstraction mechanism. The close similarity of the CO_2 vibrational distributions from reaction 4 and the decomposition of acetic acid formed by $H + CH_2C(O)OH$ allows us to conclude that the reaction proceeds through the addition of OH to acetyl radical followed by the decomposition of the acetic acid with an excitation energy of about 110 kcal mol^{-1}. Another argument for the addition/elimination mechanism is that the H_2O (or HOD) stretching excitation higher than $v_{1,3}$ (or v_3) = 3 was not observed from the spectra acquired for conditions that were favorable for reaction 4. If direct abstraction took place, the vibrational excitation in water would extend to 70 kcal mol^{-1}, giving stretching excitation as high as $v = 7$. The same situation was found for the $OH + HCO$ reaction; i.e., no emission from v_3 or $v_{1,3} > 3$ was observed for conditions in which this secondary reaction occurred. We conclude that, for both OH(OD) + HCO and OH(OD) + CH_3CO reactions, the vibrational distributions of the water product provide evidence against the direct abstraction because the combined primary and secondary H_2O and HOD spectra show no emission from $v_{1,3}$ or $v_3 \geq 4$.

The $H + CH_3CO$ (8) reaction is expected to proceed via the association of an H atom with acetyl radical, forming the activated acetaldehyde molecule, which can decompose in different ways (8a−c) or be stabilized (8d).[12,13] From the theoretical study of the unimolecular dissociation of $CH_3C(O)H$, it is known that the barrier for the production of molecular CO and CH_4, ∼85 kcal mol^{-1},[20] is nearly equal to the energy released by addition of an H atom to acetyl radical, ∼88 kcal mol^{-1}. The energetic situation is similar to that for the H + HCO reaction, where a barrier of 82 kcal mol^{-1} must be overcome to produce $H_2 + CO$ with a total energy of 86.5 kcal mol^{-1}. For CH_2O, the elimination of H_2 is the only pathway. However, the dominant path for the decomposition of $CH_3C(O)H$ gives $CH_3 + HCO$.

Another possibility to explain CO observation is decomposition of HCO from reaction 8a to H + CO. Such a reaction sequence giving vibrationally excited CO was found in the study of the analogous unimolecular reaction dynamics of chemically activated $CH_3C(O)Cl$ and $CFH_2C(O)Cl$, where initial decomposition forming ClCO was followed by the $ClCO \rightarrow Cl + CO$ process.[27] However, in the case of reaction 8a the available energy is only about 4 kcal mol^{-1} as calculated from the heats of formation of the reagents and the products. This energy is insufficient for the cleavage of the H−CO bond, $D_0(H{-}CO) = 15$ kcal mol^{-1}.[28] Thus, the observation of CO in the present study should be due to the reaction sequence 8a and 9.

5. Conclusions

The nascent vibrational distributions of H_2O and HOD molecules from OH or OD reactions with acetaldehyde have been determined from their infrared chemiluminescent spectra. The ν_3(O−H) stretching distribution of HOD is inverted with a maximum for $v_3 = 1$. The overall release of energy to the vibrational modes of the water molecule is $\langle f_v \rangle \cong 0.52$ with 30% disposed to the bending vibration and 65% disposed to the newly formed O−H bond. This energy disposal is similar to that of the reaction with formaldehyde but differs from that for reactions with *n*-butane and cyclohexane; the latter release more energy to stretching vibrations (∼80%) and less to bendings (<20%). A correlation between the $\langle E_{v_2} \rangle / \langle E_v \rangle$ and reaction rate constant can be identified.

The present study confirmed that reactions of NO_2, OH, and H with CH_3CO proceed by addition/dissociation pathways. For the $CH_3CO + NO_2$ reaction, the chemiluminescence from CO_2 molecules was observed from the $\Delta v_3 = -1$ transitions. The vibrational bending excitation of CO_2 from the unimolecular decomposition of the CH_3CO_2 radical produced via the $CH_3C(O)ONO$ intermediate extends to $v_2 = 10$ with a peak on $v_2 = 1$. This vibrational distribution is similar to that from the HCO + NO_2 reaction, e.g., to the unimolecular decomposition of the HCO_2 radical.

References and Notes

(1) Butkovskaya, N. I.; Setser, D. W. *J. Chem. Phys*. **1998**, *108*, 2434.

(2) Butkovskaya, N. I.; Setser, D. W. *J. Phys. Chem*. **1996**, *100*, 4853.

(3) Butkovskaya, N. I.; Setser, D. W. *J. Chem. Phys*. **1997**, *106*, 5028.

(4) Butkovskaya, N. I.; Setser, D. W. *J. Phys. Chem. A* **1998**, *102*, 6395.

(5) Hucknall, D. J. *Chemistry of Hydrocarbon Combustion*; Chapman & Hall: New York, 1985.

(6) Finlayson-Pitts, B. J.; Pitts, J. N., Jr. *Atmospheric Chemistry: Fundamentals and Experimental Techniques*; Wiley: New York, 1986.
(7) Butkovskaya, N. I.; Setser, D. W. *J. Phys. Chem*. **1998**, *102*, 9715.
(8) DeMore, W. B.; Golden, D. M.; Hampson, R. F.; Howard, C. J.; Kolb, C. E.; Kurylo, M. J.; Molina, M. J.; Ravishankara, A. R.; Sander, S. P. JPL Publication 92-20; **1992**; Vol. 20.
(9) Slagle, I. R.; Gutman, D. *J. Am. Chem. Soc*. **1982**, *104*, 4741.
(10) Tsang, W.; Hampson, R. F. *J. Phys. Chem. Ref. Data* **1986**, *15*, 1087.
(11) Sehested, J.; Christensen, L. K.; Nielsen, O. J.; Wallington, T. J. *Int. J. Chem. Kinet*. **1998**, *30*, 913.
(12) Bartels, M.; Edelbuttel-Einhaus, J.; Hoyermann, K. *Symp. Int. Combust. Proc*. **1991**, *23*, 131.
(13) Ohmori, K.; Miyoshi, A.; Matsui, H.; Washida, N. *J. Phys. Chem*. **1990**, *94*, 3253.
(14) Berkowitz, J.; Ellison, G. B.; Gutman, D. *J. Phys. Chem*. **1994**, *98*, 2744.
(15) Rengarajan, R.; Setser, D. W.; DesMarteau, D. *J. Phys. Chem*. **1994**, *98*, 10568.
(16) Butkovskaya, N. I.; Manke, G., II; Setser, D. W. *J. Phys. Chem*. **1995**, *99*, 11115.
(17) Nguyen, M. T.; Sengupta, D.; Raspoet, G.; Vanquickenborne, L. G. *J. Phys. Chem*. **1995**, *99*, 11883.
(18) Butkovskaya, N. I.; Muravyov, A. A.; Setser, D. W. *Chem. Phys. Lett*. **1997**, *266*, 223.
(19) von Aders, W. K.; Wagner, H. Gg. *Ber. Bunsen-Ges. Phys. Chem*. **1973**, *77*, 332.
(20) Yadav, J. S.; Goddard, J. D. *J. Chem. Phys*. **1986**, *84*, 2682.
(21) Rayez, M. T.; Scollard, D. J.; Treacy, J. J.; Sidebottom, H. W.; Balestra-Garcia, C.; Teton S.; Lebras, G. *Chem. Phys. Lett*. **1994**, *223*, 452.
(22) Francisco, J. S. *J. Chem. Soc., Faraday Trans*. **1992**, *88*, 1943.
(23) Francisco, J. S. *J. Chem. Phys*. **1992**, *96*, 7597.
(24) McKee, M. L. *J. Phys. Chem*. **1993**, *97*, 10971.
(25) Hu, W.-P.; Rosi, I., Corchado, J. C.; Truhlar, D. G. *J. Phys. Chem. A* **1997**, *101*, 6911.
(26) Butkovskaya N. I.; Setser, D. W. To be published.
(27) Srivatsava, A.; Arunan, E.; Manke, G., II; Setser, D. W.; Sumathi, R. *J. Phys. Chem*. **1998**, *102*, 6412.
(28) Becerra, R.; Carpenter, I. W.; Walsh, R. *J. Phys. Chem*. **1997**, *101*, 4185.